Nondestructive Detection of an Optical Photon

Andreas Reiserer, Stephan Ritter,* Gerhard Rempe

All optical detectors to date annihilate photons upon detection, thus excluding repeated measurements. Here, we demonstrate a robust photon detection scheme that does not rely on absorption. Instead, an incoming photon is reflected from an optical resonator containing a single atom prepared in a superposition of two states. The reflection toggles the superposition phase, which is then measured to trace the photon. Characterizing the device with faint laser pulses, a single-photon detection efficiency of 74% and a survival probability of 66% are achieved. The efficiency can be further increased by observing the photon repeatedly. The large single-photon nonlinearity of the experiment should enable the development of photonic quantum gates and the preparation of exotic quantum states of light.

More than a century ago, Planck's idea of a quantized energy exchange between light and matter and Einstein's conclusion that a light beam consists of a stream of particles have revolutionized our view of the world. The explanation of the photoelectric effect in terms of a photon-absorption process is the basis of the theoretical description of light with normally ordered photon creation and annihilation operators (*1*, *2*). The picture of photon detection as a destructive process has been confirmed experimentally ever since. Nondestructive detection (*3*)—namely, the ability to watch individual photons fly by—has until now been an unaccomplished "ultimate goal" (*4*) of optical measurements.

Nondestructive detection has two major implications. First, a single photon can be detected more than once. Thus, concatenating several devices improves the detection efficiency of single photons. Second, nondestructive detection can serve as a herald that signals the presence of a photon without affecting its other degrees of freedom, such as its temporal shape or its polarization. This is in stark contrast to absorbing detectors, in which the quantum state of the photon is projected and therefore lost. Both implications are of great importance for rapidly evolving research fields such as quantum measurement (*5*), optical quantum computing (*6*), and quantum communication and networking (*7*, *8*).

The interaction mechanism (*9*) we implement is based on the principles of cavity quantum electrodynamics, remarkably robust, and applicable to many different physical systems. It allows one to nondestructively detect propagating optical photons and thus to complement experiments with microwave fields trapped in superconducting resonators (*10*–*12*). To this end, a faint laser pulse is reflected off a resonant cavity in which a trapped atom has been prepared in a superposition of two internal states. The cavity induces strong coupling between the light pulse and the atom in one of the atomic states, but not the other. This leads to a phase flip of the atomic superposition state upon reflection of a photon. Subsequent readout of the atomic phase thus makes it possible to detect a photon without absorbing it.

A detailed theoretical treatment of the atom-photon interaction mechanism is given in (*9*, *13*). For an intuitive explanation, consider a three-level atom in a single-sided cavity (Fig. 1A) in which one of the mirrors is perfectly reflecting and the small transmission of the other mirror allows for in- and outcoupling of light. The cavity is thus overcoupled and resonant with the transition between the atomic states $|2\rangle_a$ and $|3\rangle_a$. A photon, resonant with the empty cavity, is impinging onto the transmitting mirror. If the atom is in the state $|1\rangle_a$, it will not interact with the photon because any transition is far detuned. Thus, the photon will enter the cavity before being reflected. If, however, the atom is in $|2\rangle_a$ (Fig. 1B), the strong atom-photon coupling leads to a normal-mode splitting, so that the photon is reflected without entering the cavity. In this case, atom and photon were never in the same place. Nevertheless, the photon has left a trace in the state of the atom: When light is reflected from a resonant cavity, it experiences a phase shift of π, whereas there is no phase shift in the strongly coupled case. When the impinging photon is denoted by the state $|1\rangle_p$, we thus find $|2\rangle_a|1\rangle_p \rightarrow |2\rangle_a|1\rangle_p$, whereas $|1\rangle_a|1\rangle_p \rightarrow e^{i\pi}|1\rangle_a|1\rangle_p = -|1\rangle_a|1\rangle_p$.

To use this conditional phase shift for nondestructive photon detection, the atom is prepared in the superposition state $\frac{1}{\sqrt{2}}(|1\rangle_a + |2\rangle_a)$ (Fig. 1C). If there is no impinging photon, the atomic state remains unchanged (Fig. 1D, solid green circle). If, however, a photon is reflected, the atomic state becomes (omitting a global phase) $\frac{1}{\sqrt{2}}(|1\rangle_a + |2\rangle_a)|1\rangle_p \rightarrow \frac{1}{\sqrt{2}}(|1\rangle_a - |2\rangle_a)|1\rangle_p$ (Fig. 1D, red arrow and solid red circle). To measure this phase flip, a π/2 rotation maps the atomic state $\frac{1}{\sqrt{2}}(|1\rangle_a + |2\rangle_a)$ onto $|1\rangle_a$, whereas $\frac{1}{\sqrt{2}}(|1\rangle_a - |2\rangle_a)$ is rotated to $|2\rangle_a$ (Fig. 1E). Subsequently, cavity-enhanced fluorescence state detection (*14*) is used to discriminate between the atomic states $|1\rangle_a$ and $|2\rangle_a$ (Fig. 1F) (*15*). Two photons in the input pulse lead to a phase shift of $e^{i2\pi} = 1$. The used sequence therefore measures the odd-even parity of the photon number. As long as the average photon number per measurement interval is much smaller than one, only zero or one photon events are present, and the detection result is unambiguous.

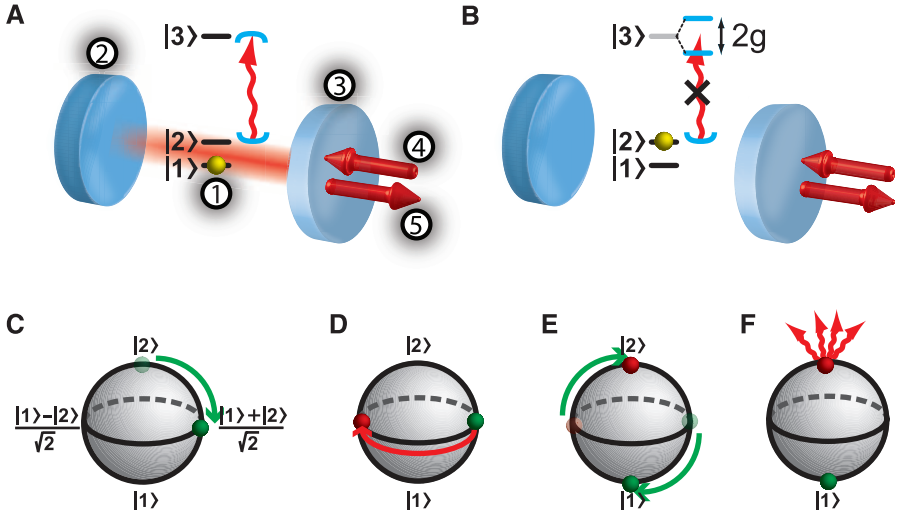

Fig. 1. Nondestructive photon detection. (**A** and **B**) Sketch of the setup and atomic level scheme. A single atom, (1), is trapped in an optical cavity that consists of a high-reflector, (2), and a coupling mirror, (3). A resonant photon is impinging on, (4), and reflected off, (5), the cavity. (**A**) If the atom is in state $|1\rangle_a$, the photon (red wavy arrow) enters the cavity (blue semicircles) before being reflected. In this process, the combined atom-photon state acquires a phase shift of π. (**B**) If the atom is in $|2\rangle_a$, the strong coupling on the $|2\rangle_a \leftrightarrow |3\rangle_a$ transition leads to a normal-mode splitting of $2g$, so that the photon cannot enter the cavity and is directly reflected without a phase shift. (**C** to **F**) Procedure to measure whether a photon has been reflected. (**C**) The atomic state, visualized on the Bloch sphere, is prepared in the superposition state $\frac{1}{\sqrt{2}}(|1\rangle_a + |2\rangle_a)$. (**D**) If a photon impinges, the atomic state is flipped to $\frac{1}{\sqrt{2}}(|1\rangle_a - |2\rangle_a)$. (**E**) The atomic state is rotated by $\frac{\pi}{2}$. (**F**) Fluorescence detection is used to discriminate between the states $|1\rangle_a$ and $|2\rangle_a$.

Max-Planck-Institut für Quantenoptik, Hans-Kopfermann-Strasse 1, 85748 Garching, Germany.

*Corresponding author. E-mail: stephan.ritter@mpq.mpg.de

In our setup (*16*), a single ^{87}Rb atom is trapped in a three-dimensional optical lattice at the center of a Fabry-Perot resonator. The coupling mirror has a transmission of 95 parts per million (ppm), which is large compared with the transmission of the high-reflector and the scattering and absorption losses (8 ppm). The cavity field decay rate is $\kappa = 2\pi \times 2.5$ MHz, the atomic dipole decay rate is $\gamma = 2\pi \times 3$ MHz, and the measured atom-cavity coupling constant on the $|2\rangle_a \leftrightarrow |3\rangle_a$ transition is $g = 2\pi \times 6.7$ MHz (*16*). Thus, the system operates in the strong-coupling regime of cavity quantum electrodynamics.

We first demonstrate that we can accurately prepare, control, and readout the atomic state. The atom is initialized in the state $|2\rangle_a$ by optical pumping, and the levels $|2\rangle_a$ and $|1\rangle_a$ are coupled by using a pair of Raman lasers (*15*). To characterize this coupling, the Raman beams were applied for a variable duration, and the population in $|2\rangle_a$ was measured (*14*, *15*). Observing Rabi oscillations (Fig. 2A) with a visibility of 97% represents an upper bound for the quality of our state preparation, rotation, and readout process.

Strong coupling between the atom and impinging light is demonstrated by measuring the reflection of the system with the atom prepared in $|2\rangle_a$ as a function of the probe light frequency (Fig. 2B, red data). The observed normal-mode splitting testifies to the strong coupling. On resonance, 62(2)% of the impinging photons are reflected (with the number in parentheses being the statistical SE). With increasing coupling strength, this value is expected to approach unity. When the atom is prepared in the uncoupled state $|1\rangle_a$, 70(2)% of the incoming light is reflected on resonance (Fig. 2B, black data). The missing 30% are either transmitted through the high reflector or lost via scattering or absorption, which is in good agreement with input-output theory calculations (*17*) when using the independently measured mirror parameters.

Having characterized the individual steps of the protocol, they are now combined to detect photons in a nondestructive way. The atom is prepared in the superposition state $\frac{1}{\sqrt{2}}(|1\rangle_a + |2\rangle_a)$. Within a 2.5-μs-long trigger interval, we sent in a weak coherent laser pulse with an average photon number of $\bar{n} = 0.115(11)$ and monitor its reflection with conventional single-photon counting modules (SPCMs). A typical experimental run is shown in Fig. 3A, in which a photon was subsequently detected (red line in the blue trigger interval). Therefore, after π/2 rotation of the atomic state many fluorescence photons are observed (*14*) in the 25-μs-long readout interval (gray), unambiguously signaling the atomic state change induced by the detected photon. Thus, in the case shown in Fig. 3A a photon is detected twice: by the nondestructive detector and with a conventional, absorptive SPCM. The depicted trace also indicates that the setup works as an all-optical switch (*18*) that does not destroy the impinging trigger photon and also does not affect its temporal envelope. The latter can be seen in Fig. 3B, in which the arrival-time histogram of the photons detected with the SPCMs after reflection from the setup is shown. The data taken during the nondestructive photon measurement (Fig. 3B, black squares) do not show a clear deviation from the reference curve recorded without atom (Fig. 3B, red points)—except for a small reduction in amplitude, which is consistent with the results of Fig. 2B.

When the input pulse is blocked, no photons are observed, neither in the blue nor in the gray interval of Fig. 3A, in 97.1(4)% of all runs. In the remaining 2.9%, many fluorescence photons are observed during the atomic state readout, corresponding to a "dark count" of the nondestructive photon detector. This is caused by imperfections in the atomic state preparation, rotation, and readout and might be improved by magnetic shielding of the setup and by using more complex state-rotation techniques, such as composite pulses (*19*).

We then investigated the photon detection efficiency of our nondestructive device. The probability of detecting a photon in the input pulse is given in Fig. 3C. The results obtained with calibrated conventional SPCMs, without and with correction for their limited quantum efficiency of 55(5)%, are shown as yellow and gray bars, respectively. The red bars are obtained from the atomic-state readout. Comparison of the gray and red bars shows good agreement but does not reveal information about potential systematic errors. Therefore, we also analyzed correlations between the detection of a reflected photon by the SPCMs and by our nondestructive detector. The blue bars show the probability of finding the atom in $|2\rangle_a$, conditioned on the detection of a photon by the SPCMs. We obtained 82.1(1.7)%. Correcting for the influence of two-photon components in the input laser field (and SPCM dark counts) (*15*), the conditional detection efficiency of our device for single photons is 87%.

There are two major experimental imperfections (*15*) that contribute to the deviation of the conditional detection efficiency from unity. First, the spatial mode matching of the input photons and the cavity mode [92(2)%; corresponding reduction 12(3)%], and second, the fidelity of the atomic state preparation, rotation, and readout (estimated reduction 3%) (*15*). None of the imperfections has a fundamental limit. Therefore, it should be possible to further increase the ef-

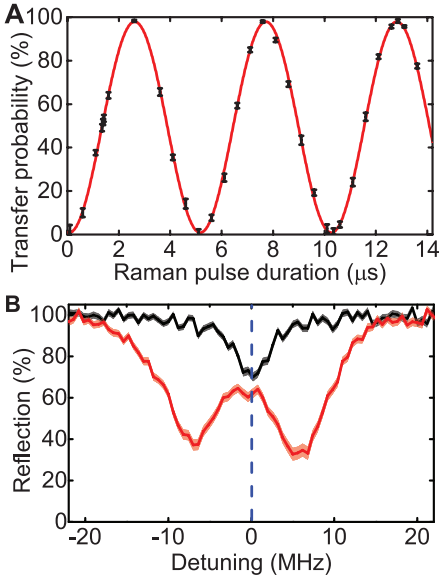

Fig. 2. Atomic state manipulation and cavity reflection spectrum. (**A**) Rabi oscillations of the atomic population when the atom is prepared in $|2\rangle_a$, and two Raman laser beams are applied for a variable duration. The red fit curve gives a visibility of 97%. (**B**) Reflection off the atom-cavity system as a function of probe laser frequency, with the atom in the strongly coupled state $|2\rangle_a$ (red) or in the uncoupled state $|1\rangle_a$ (black). The statistical SE is given by the thickness of the lines.

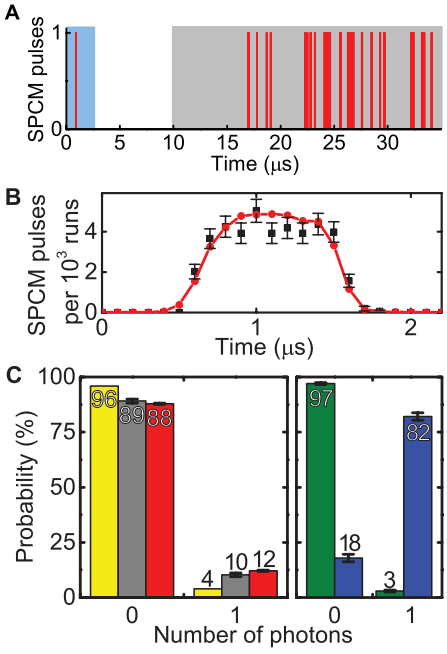

Fig. 3. Experimental results. (**A**) Typical trace of an experimental run. A photon (red bar) impinging in the trigger interval (blue area) leads to the emission of many photons in the readout interval (gray area). When the input pulse is blocked, no photons are detected in both intervals. (**B**) Temporal envelope of the reflected photon pulse when an atom is present (black squares) compared with a reference run without atom (red points). Within the errors, no deviation in the pulse shape is observable, except for a small amplitude change stemming from the slightly different reflectivities (Fig. 2B). (**C**) Nondestructive detection of a single photon. The probability of detecting zero or one photon is plotted. Yellow, result of the SPCM detection; gray, calculated input pulse, taking into account the SPCM detection efficiency; red, result of the atomic state readout; green, atomic state readout without impinging light; blue, atomic state, conditioned on the SPCM detection of a reflected photon in the trigger interval.

ficiency achieved in our first proof-of-principle experiment, which already compares well with state-of-the-art absorbing single-photon detectors (*20*–*22*).

The probability that an impinging photon is reflected is on average 66(2)%. If a photon is absorbed, the atomic state is projected, and the detection process gives the wrong result with a probability of 50%. Therefore, the probability to detect a single input photon without postselection on its reflection from the cavity is calculated to be 74% (*15*).

In contrast to all absorbing detectors, the efficiency of our detector can be further improved by attempting more measurements. Concatenating two of our devices is expected to increase the detection efficiency to 87%, whereas three or more devices should yield 89% (*15*). The achieved value is currently limited by absorption and scattering losses of both the atom and the cavity mirrors. To further improve, a decrease in cavity loss or an increase in atom-cavity coupling strength would be required. Both can be achieved either in Fabry-Perot (*23*) or other (*24*–*26*) resonators.

The atom-photon interaction mechanism that has been presented in this work lays the ground work for numerous experiments. A first step is the repeated nondestructive measurement of a single optical photon. Next, with a higher number of photons in the impinging laser pulse, the odd-even parity measurement allows one to generate new quantum states of optical light fields, such as Schrödinger-cat states (*27*). Measuring the phase of the reflected light could be used to entangle two atoms in the cavity (*28*). Moreover, using the polarization degree of freedom as a qubit should facilitate a deterministic quantum gate between a single photon and a single atom (*9*, *13*). This can be further extended to an entangling gate between several successively impinging photons (*9*) or between several atoms trapped in the same or even in remote cavities, thus efficiently generating atomic cluster states (*13*, *29*, *30*). Implementing this gate operation would also allow for a deterministic photonic Bell-state measurement, which would increase the efficiency of measurement-based quantum networks with remote single atoms (*31*, *32*) close to unity.

References and Notes

1. R. J. Glauber, *Phys. Rev.* **130**, 2529–2539 (1963).
2. L. Mandel, E. Wolf, *Optical Coherence and Quantum Optics* (Cambridge Univ. Press, Cambridge, 1995).
3. V. B. Braginsky, F. Y. Khalili, *Rev. Mod. Phys.* **68**, 1–11 (1996).
4. P. Grangier, J. A. Levenson, J.-P. Poizat, *Nature* **396**, 537–542 (1998).
5. H. M. Wiseman, G. J. Milburn, *Quantum Measurement and Control* (Cambridge Univ. Press, Cambridge, 2009).
6. J. L. O'Brien, *Science* **318**, 1567–1570 (2007).
7. N. Gisin, R. Thew, *Nat. Photonics* **1**, 165–171 (2007).
8. H. J. Kimble, *Nature* **453**, 1023–1030 (2008).
9. L.-M. Duan, H. J. Kimble, *Phys. Rev. Lett.* **92**, 127902 (2004).
10. G. Nogues *et al.*, *Nature* **400**, 239–242 (1999).
11. C. Guerlin *et al.*, *Nature* **448**, 889–893 (2007).
12. B. R. Johnson *et al.*, *Nat. Phys.* **6**, 663–667 (2010).
13. J. Cho, H.-W. Lee, *Phys. Rev. Lett.* **95**, 160501 (2005).
14. J. Bochmann *et al.*, *Phys. Rev. Lett.* **104**, 203601 (2010).
15. Materials and methods are available as supplementary materials on *Science* Online.
16. A. Reiserer, C. Nölleke, S. Ritter, G. Rempe, *Phys. Rev. Lett.* **110**, 223003 (2013).
17. D. F. Walls, G. J. Milburn, *Quantum Optics* (Springer, 2008).
18. W. Chen *et al.*, *Science* **341**, 768–770 (2013).
19. L. M. K. Vandersypen, I. L. Chuang, *Rev. Mod. Phys.* **76**, 1037–1069 (2005).
20. R. H. Hadfield, *Nat. Photonics* **3**, 696–705 (2009).
21. M. D. Eisaman, J. Fan, A. Migdall, S. V. Polyakov, *Rev. Sci. Instrum.* **82**, 071101 (2011).
22. F. Marsili *et al.*, *Nat. Photonics* **7**, 210–214 (2013).
23. Y. Colombe *et al.*, *Nature* **450**, 272–276 (2007).
24. B. Dayan *et al.*, *Science* **319**, 1062–1065 (2008).
25. C. Junge, D. O'Shea, J. Volz, A. Rauschenbeutel, *Phys. Rev. Lett.* **110**, 213604 (2013).
26. J. D. Thompson *et al.*, *Science* **340**, 1202–1205 (2013).
27. B. Wang, L.-M. Duan, *Phys. Rev. A* **72**, 022320 (2005).
28. A. S. Sørensen, K. Mølmer, *Phys. Rev. Lett.* **91**, 097905 (2003).
29. Y.-F. Xiao *et al.*, *Phys. Rev. A* **70**, 042314 (2004).
30. L.-M. Duan, B. Wang, H. J. Kimble, *Phys. Rev. A* **72**, 032333 (2005).
31. D. L. Moehring *et al.*, *Nature* **449**, 68–71 (2007).
32. C. Nölleke *et al.*, *Phys. Rev. Lett.* **110**, 140403 (2013).

Acknowledgments: We thank N. Kalb for experimental assistance. This work was supported by the European Union (Collaborative Project SIQS) and the Bundesministerium für Bildung und Forschung via IKT 2020 (QK_QuOReP).

Supplementary Materials

www.sciencemag.org/content/342/6164/1349/suppl/DC1
Materials and Methods
Fig. S1

18 September 2013; accepted 5 November 2013
Published online 14 November 2013;
10.1126/science.1246164

Effect of Collective Molecular Reorientations on Brownian Motion of Colloids in Nematic Liquid Crystal

T. Turiv,[1,2] I. Lazo,[2] A. Brodin,[1,3] B. I. Lev,[4] V. Reiffenrath,[5] V. G. Nazarenko,[1] O. D. Lavrentovich[2]*

In the simplest realization of Brownian motion, a colloidal sphere moves randomly in an isotropic fluid; its mean squared displacement (MSD) grows linearly with time τ. Brownian motion in an orientationally ordered fluid—a nematic—is anisotropic, with the MSD being larger along the axis of molecular orientation, called the director. We found that at short time scales, the anisotropic diffusion in a nematic becomes anomalous, with the MSD growing slower or faster than τ; these states are respectively termed subdiffusion and superdiffusion. The anomalous diffusion occurs at time scales that correspond to the relaxation times of director deformations around the sphere. Once the nematic melts, the diffusion becomes normal and isotropic. Our experiment shows that the deformations and fluctuations of long-range orientational order profoundly influence diffusive regimes.

Random displacements of a small particle in a fluid are controlled by kinetic energy dissipation (*1*). The mean displacement is zero but the average mean squared displacement (MSD) is finite, growing linearly with time lag τ (*2*): $\langle \Delta \mathbf{r}^2(\tau) \rangle = 6D\tau$, where D is the translational diffusion coefficient. Brownian particles in complex fluids may exhibit an anomalous behavior, $\langle \Delta \mathbf{r}^2(\tau) \rangle \propto \tau^{\alpha}$, with the exponent α either smaller than 1 (subdiffusion) or larger than 1 (superdiffusion). Subdiffusion is observed in polymer (*3*) and F-actin networks (*4*) and in surfactant dispersions (*5*); superdiffusion occurs in concentrated suspensions of swimming bacteria (*6*) and dispersions of polymer-like micelles (*7*–*10*). The diffusion regimes should reflect the properties of the host medium (*11*), one of which is often a local or long-range orientational order of molecules.

The simplest orientationally ordered fluid is a uniaxial nematic, in which the average orientation of molecules is described by a unit director $\hat{\mathbf{n}}$. Because of different effective viscosities $\eta_{\parallel} \neq \eta_{\perp}$ for motion parallel and perpendicular to $\hat{\mathbf{n}}$, Brownian motion becomes anisotropic, with two coefficients $D_{\parallel}$ and $D_{\perp}$ (*12*–*19*). The anisotropic diffusion characterized experimentally to date for nematics at relatively long time lags τ remains "normal," with $\alpha = 1$ (*14*–*19*). In some cases, anomalous diffusion has also been observed, but it was attributed to features other than the orientational order, such as bacterial activity (*6*), size distribution of building units (*7*), spatial modulation of hydrophobic and hydrophilic regions (*8*), bending rigidity of the molecular aggregates (*8*), fluctuations of concentration (*9*), or director distortions around the dye molecules (*20*). Here, we show that the nematic orientational order and its

[1]Institute of Physics NASU, Prospect Nauky 46, Kyiv 03039, Ukraine. [2]Liquid Crystal Institute, Kent State University, Kent, OH 44242, USA. [3]National Technical University of Ukraine "KPI," Prospect Peremogy 37, Kyiv 03056, Ukraine. [4]Bogolyubov Institute for Theoretical Physics NASU, 14-b Metrolohichna Street, Kyiv 03680, Ukraine. [5]Liquid Crystals Division, Merck KGaA, 64271 Darmstadt, Germany.

*Corresponding author. E-mail: olavrent@kent.edu